



Cite this: *Phys. Chem. Chem. Phys.*,
2017, **19**, 19699

Received 17th March 2017,
Accepted 8th May 2017

DOI: 10.1039/c7cp01705g

rsc.li/pccp

Single photon transient hot electron ionization of C₆₀

K. Hansen ^{ab}

Recent experiments have demonstrated that C₆₀ can ionize in a thermal process after absorption of a photon with energy far above the ionization energy. This indirect ionization mechanism is investigated here by calculating the total and singly charged ion yields, electron energy distributions, and effective electronic temperatures as a function of photon energy.

1 Introduction

Photo ionization of molecules can proceed *via* several different mechanisms. The best known is the direct photo ionization, where the absorption of a single photon above the ionization threshold produces an ion and an electron with a kinetic energy that corresponds to the photon energy minus the binding energy of the level of the origin of the electron (see *e.g.* ref. 1 and 2). Single photon absorption may also initiate Auger electron emission processes, either upon resonant excitation of the neutral system or in combination with primary direct ionization of an inner shell (see *e.g.* ref. 3). Multi-photon ionization may occur *via* the so-called above threshold ionization (ATI) (see *e.g.* ref. 4–6 and references therein), wherein the strong electric field of a laser pulse shifts levels into resonance with the photon energies and provides a ladder for multiple absorption of photons that ultimately results in the emission of an electron.

In contrast, a much more indirect type of ionization has been observed after multi-photon absorption of photons below the ionization energy in a process which is the nano-scale analogue of the bulk thermionic emission.^{7–9} This ionization mechanism does not depend on the precise excitation mechanism and will also appear after, *e.g.*, collisional excitation. The main requirement for the occurrence of this type of ionization is that the threshold for thermally activated electron emission, which is the adiabatic ionization energy, is below the activation energy for the competing process of thermal emission of atoms or small molecules by 30% or more.¹⁰

Yet another type of ionization has been observed in Penning ionization of the fullerenes C₆₀ and C₇₀^{11,12} and in experiments employing sub-ps laser pulses with photon energies far below the ionization energy, both on these two fullerenes^{13,14} and on metal clusters.^{15–17} The primary distinguishing feature of this ionization is the smooth and featureless low energy electron spectrum.¹⁸ The spectra are essentially exponential and are interpreted as thermal spectra. The characteristic energy of the exponential is given by the temperature of the emitting species, the product electronic temperature, to be precise. For comparison, the likewise high-intensity laser pulse ATI processes produce a series of peaks at energies corresponding to the number of absorbed photons minus the ionization energy.¹³ Work on polycyclic aromatic hydrocarbon (PAH) molecules has extended the range downward in the size of the molecules from the initially measured C₆₀.¹⁹ Also rare gas clusters have been observed to display the phenomenon in experiments with multiple high energy photon absorption.²⁰

The simple form of the observed electron spectra is a consequence of the special features of the pre-exponential factors of the rate constant. These arise as a consequence of the Coulomb potential which the emitted electron traverses on the way out of the molecule, as will be clear when the explicit expression for the rate constant is discussed below. In connection with the thermal process, the effect of this potential is fortuitous. The kinetic energy releases from unimolecular decays, for comparison, usually display a peak at a non-zero energy, in spite of the fact that these distributions are also thermal in nature. The shape of the distributions of electrons emitted in a process where the product is a positive ion nevertheless gives the emission temperature rather directly to a good approximation.¹⁸

The temperatures fitted from these experimental curves are very high, on the order of an electronvolt (1 eV = 11 605 K).^{14,18,19} Such values correspond very well to the expected temperatures

^a Tianjin International Center of Nanoparticles and Nanosystems, Tianjin University, 92 Weijin Road, Nankai district, Tianjin 300072, P. R. China. E-mail: KlavsHansen@tju.edu.cn

^b Department of Physics, University of Gothenburg, 41296 Gothenburg, Sweden

The quantitative analysis will give quantum ionization yields and kinetic energy spectra. The main unknown that will remain unknown until further development of the theory is the precise mechanism of photon absorption. The creation of the hot electron gas will be treated as an experimental fact in this work.

2 Experimental background

The experimental procedure and equipment has been described in detail in ref. 26 and references therein, and since this work is primarily concerned with theoretical predictions, only a brief overview, sufficient to motivate the calculations, will be given here. The experiments were performed at the gas phase beamline³⁰ at the Elettra synchrotron radiation facility. The electron spectra were recorded using a velocity map imaging spectrometer (VMI),³¹ with the light polarized parallel to the detector plane. This allows the rotationally symmetric 3-d distribution of velocities emitted during the ionization to be reconstructed from the measured two-dimensional data.^{32,33}

The electrons were measured in coincidence with ions which were mass analyzed using a time-of-flight mass spectrometer mounted back-to-back with the VMI.³⁰ The setup allows us to assign individual electrons to the molecule they originate from. The intensity of the light was kept low to avoid false coincidences, mainly from the residual gas in the chamber. The light intensity was therefore so low that effects of strong fields were absent. Spectra were measured for single ionization of C_{60} , producing C_{60}^+ parent ions or the fragment ions C_{58}^+ and C_{56}^+ .

At sufficiently high energies, C_2 loss from C_{60}^+ was observed. This loss sets in at the energy previously observed in energy resolved collision induced fragmentation experiments and occurs on much longer time scales, closer to the time scale of our mass spectrometer, than the sub-ps relevant for the initial ionization. The electron spectra measured in coincidence with C_{58}^+ and C_{56}^+ therefore also originate from ionization of C_{60} and can be used on an equal footing with the spectra for which the coincidence ion is the ionized, intact parent molecule. These fragment spectra even have the advantage that the background from direct processes that may be present for C_{60}^- are absent, and the spectra are therefore effectively background-free.

3 Observables

As already mentioned, the electron energy distributions are expected to be close to exponential, with a characteristic energy that corresponds to the effective emission temperature. As for all thermal emission processes, this temperature is that of the product, *i.e.* the electron temperature of C_{60}^+ here. The precise form follows from the Weisskopf rate constant applied to electron emission:²⁴

$$k(E, \varepsilon) d\varepsilon = \frac{2m_e \sigma(\varepsilon) \rho_d(E - \Phi - \varepsilon)}{\pi^2 \hbar^3} \frac{\rho_p(E)}{\rho_p(E)} d\varepsilon. \quad (1)$$

Here ε is the kinetic energy of the electron, m_e the mass of the electron (in principle the reduced mass of the channel), ρ the

level density and Φ the ionization energy. The value of Φ is $\Phi_1 = 7.6$ eV for the first ionization and $\Phi_2 = 11.4$ eV for the second. The factor of two in eqn (1) is the spin degeneracy of the electron and $\sigma(\varepsilon)$ is the capture cross section for an electron in the Coulomb potential of the daughter. The ρ values are the electronic level densities of C_{60} and C_{60}^+ , as indicated by the subscripts p and d, respectively, for parent and daughter.

The application of the Weisskopf theory to describe electron emission after absorption of a single photon is justified by the experimental data. Weisskopf theory, or in more general detailed balance, is the general theoretical framework of the quantitative description of thermal emission processes, and the conclusion from the experimental data, together with data previously measured with multiphoton processes, is that the decay process after multiphoton and single photon absorption is the same, and produced in a (quasi-)thermal process. The great surprise here is that the single photon and the multiphoton excitation processes also appear to have very similar features, *viz.* the creation of the hot electron system.

Level densities are generally defined as the number of quantum states per energy interval. Apart from a multiplicative parameter of dimension reciprocal energy, they are essentially equal to the exponentials of the canonical entropy. Expansion of the logarithm of the ion level density in the excitation energy gives

$$f(E, \varepsilon) = c' \sigma(\varepsilon) \varepsilon \rho_d(E - \Phi) \approx c \sigma(\varepsilon) \varepsilon e^{-\varepsilon/T_e}, \quad (2)$$

where T_e is defined as

$$T_e^{-1} = \frac{d \ln \rho_c(E)}{dE}, \quad (3)$$

in close analogy to the canonical Maxwell relation for the corresponding quantities. The two constants c' and c ensure normalization to unit probability. The approximation in the last equality in eqn (2) provides a useful picture for a heuristic understanding of the distributions. In particular we see that if $\varepsilon \sigma(\varepsilon)$ is a constant, which will be argued shortly, the distribution will be Boltzmannian. In the simulations, however, the energy distributions will be calculated directly from the level densities. The total ionization rate is

$$k(E) = \int_0^E k(E, \varepsilon) d\varepsilon = \frac{2m_e}{\pi^2 \hbar^3 \rho_p(E)} \int_0^E \varepsilon \sigma(\varepsilon) \rho_d(E - \Phi - \varepsilon) d\varepsilon. \quad (4)$$

The level densities are calculated with the use of the single particle spectrum from a Local Density Approximation calculation of Yabana,³⁴ with all the caveats one must face when using this type of calculation for an excited state calculation. The single particle spectra of the two cations relevant for this work were taken to be identical to that of the neutral. The details of the calculation converting the single particle levels to total system density of states are given in ref. 18, and are similar to the technique given in ref. 35 and in the context of equilibrated clusters also in ref. 36. As in ref. 18, we will use a level density slightly modified relative to this calculation, *viz.* the form $\rho_d(E) = \rho_{d,calc}(E)^{1.12} / \rho_{d,calc}(20 \text{ eV})^{0.12}$ for both the neutral and the ion level densities. The calculated level density is

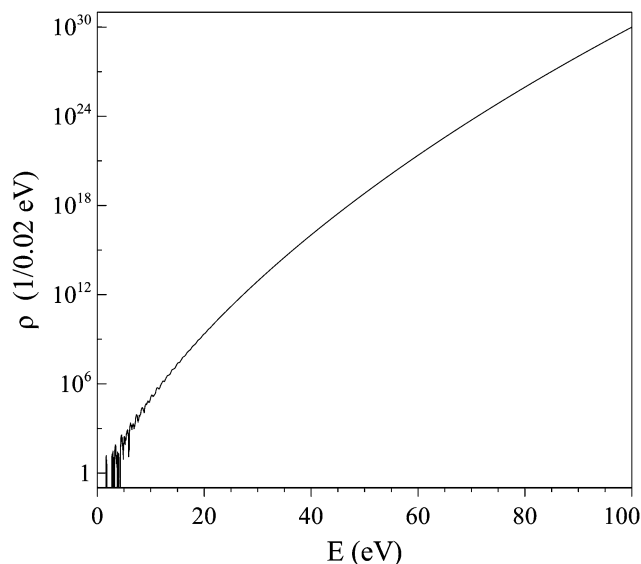


Fig. 1 The calculated level density for the electronic excitations, as a function of excitation energy. The unit is the reciprocal discretization energy of 0.02 eV in the calculation of the quantity.

shown in Fig. 1. The resulting rate constants for the first and second ionization, k_0 and k_1 respectively, are shown in Fig. 2.

Two factors need to be considered when comparing the experimentally observed energy distributions with eqn (2). One is that the electron capture cross section is strongly energy dependent for capture in a Coulomb potential. We will use the classical value with capture on contact, which is $\sigma = (1 + 3.0 \text{ eV}/\varepsilon)\sigma_{\text{geo}}$, where σ_{geo} is the cross section corresponding to the contact radius. The second factor, which is of lesser importance numerically, is that the electronic excitation energy, and hence the emission temperature, is not constant with time. For electrons emitted from the

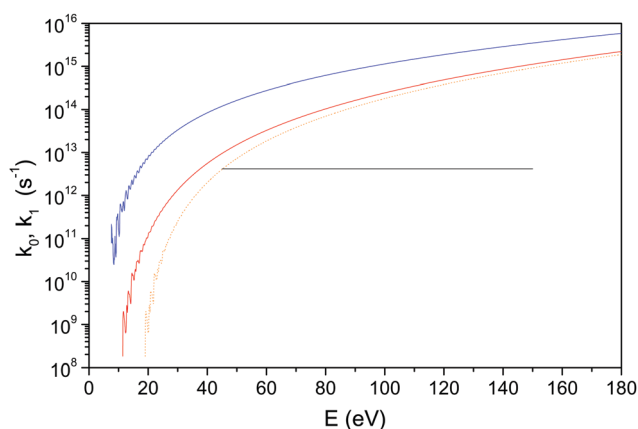


Fig. 2 The rate constants for the first and second ionizations (top, blue curve and second from top, red, respectively) vs. excitation energy. The dotted, orange line shows the second ionization rate constant shifted up in energy by the first ionization energy. This curve therefore gives the second ionization rate constant vs. photon energy. The horizontal line is the reciprocal of the 240 fs coupling time. It crosses the dotted line at 45 eV, indicating the onset of the second ionization around this excitation energy.

neutral molecule, it varies from the maximum $h\nu - \Phi$, where $\Phi = 7.6 \text{ eV}$ is the first ionization energy, to zero when the electronic excitation falls below Φ . We will use a simple exponential decrease to describe the dissipation of electronic energy into the vibrational manifold,

$$E = E(0)e^{-t/\tau}, \quad (5)$$

with the fitted value of 240 fs for τ .

Thermal loss of more than one electron is possible. For the higher charge states, the rate constant can be calculated in analogy to the rate constant for the first ionization, employing the relevant level densities and activation energies in eqn (1) and changing the cross section, for which the value 3.0 eV is replaced by $3.0q \text{ eV}$, with q the charge of the final state.

The calculation here is similar to the one presented in ref. 18, where the yield and electron energy distributions are calculated for near infrared photon absorption, with respect to the rate constant, the kinetic energy distributions and the electron excitation energy dissipation. The main difference is the photon statistics. With a reaction induced by a single photon, the summation over the assumed Poisson statistics of the absorbed photon numbers and the integration over varying laser intensities across space become irrelevant. An additional difference is that the delta-function time-dependence of the electronic excitation in the single photon absorption case treated here is a better approximation to the physical situation, although it should be kept in mind that the establishment of the electronic excitation will still take a finite, albeit short, time. With respect to the excitation energies delivered to the fullerene, the experiments are therefore similar to the Penning ionization experiments¹¹ that triggered the development of the model originally. Two important differences are that in the synchrotron light experiments the energy can be varied continuously, and that the electron spectra were measured here.

With the exponential equilibration time dependence, the neutral molecule population, P_0 , after time t is given by

$$P_0(t) = P_0(0) \exp\left(-\int_0^t k_0(h\nu e^{-t'/\tau}) dt'\right). \quad (6)$$

The total ionization yield, *i.e.* the complementary of this function, $1 - P_0$, is shown in Fig. 3 for several different photon energies as a function of time. The initial increase with the slope proportional to time is interrupted before 10^{-13} s for low photon energies, and earlier for the high energies, where the effects of depletion of the neutral molecule depletes the population and the flattening of the curve occurs before the quenching of the electronic motion has occurred.

Although the curves in Fig. 3 are shown to start at 1 fs, and the electron–electron equilibration time is expected to be fairly short, two caveats must be given for a too literal interpretation of the calculations involving these short times. One is the fact that it takes a finite time for the electron to leave the fullerene. For a typical electron kinetic energy of 1 eV, it takes 0.6 fs to move the distance of 3.5 Å that corresponds to the radius of the nuclear cage of C_{60} . The other is that, incidentally, energies and times of the magnitude combine to an action close to Planck's

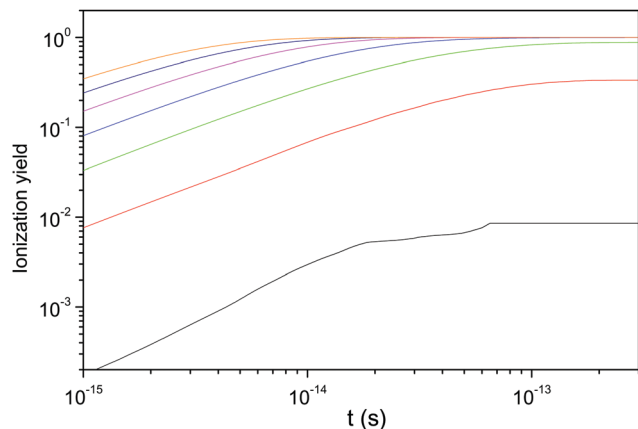


Fig. 3 The fraction of C_{60} molecules that have ionized at least once, as a function of time. The photon energies are 10 eV (black line), 20 eV (red line), 30 eV (green line), 40 eV (blue line), 50 eV (magenta line), 60 eV (navy line), and 70 eV (orange line). The values are quantum yields for the hot electron ionization, *i.e.* the values are normalized to the number of molecules that have absorbed a photon but not ionized in a direct process. Fragments and higher charge states are included in the ion count here.

constant ($\hbar = 0.66$ eV fs). The precise implications of the latter fact for the rate constants at high excitation energies are presently not clear.

Fig. 4 shows the ionization yield at asymptotically long times as a function of photon energy. Also here are all charge states with $q > 0$ and all fragments included.

Fig. 5 shows the emission rate *vs.* time for the same photon energies, *i.e.* the product $P_0(t)k_0(t)$. This continues to decrease with time due to the continued decrease in electronic excitation energy that reduces k also for times where P is essentially frozen.

Ionization events involving a second or third ionization are not detected in the experiments because only a single electron can be detected energy-resolved in each event. The detected signal in these experiments is therefore proportional to the

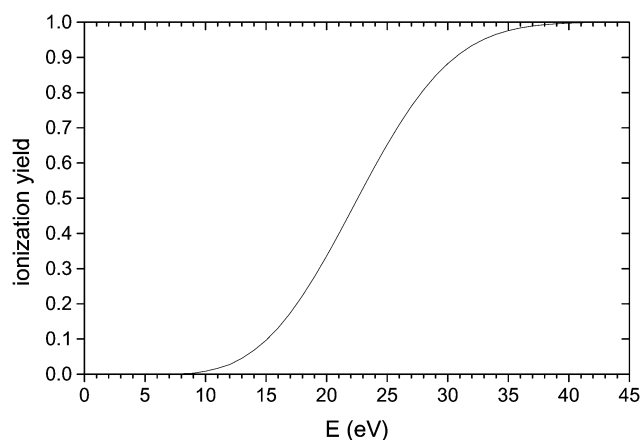


Fig. 4 Ionization yield, calculated with eqn (6), corresponding to the total quantum ion yield for the molecules that absorb a photon and do not ionize directly. This represents the sum of all charged species exclusive of the directly ionized.

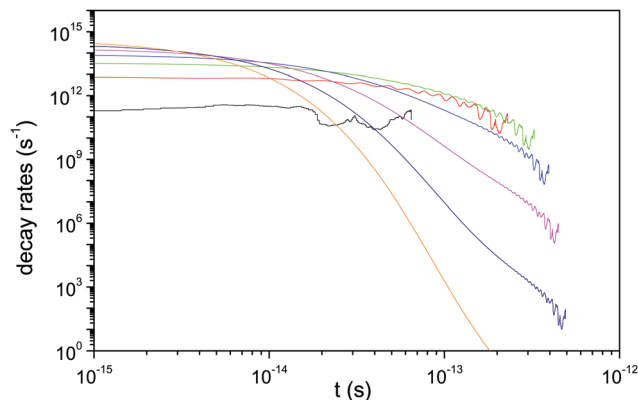


Fig. 5 The emission rate, k_0P_0 , for hot electron ionization of C_{60} for the same photon energies as shown in Fig. 3, 10 eV (black line), 20 eV (red line), 30 eV (green line), 40 eV (blue line), 50 eV (magenta line), 60 eV (navy line), and 70 eV (orange line). The curves terminate when the energy decreases below 7.6 eV. The wiggles on the curves at long times are due to the non-smooth electronic level densities of the ion close to the ground state.

population of the singly charged cation, P_1 . Semiquantitative considerations indicate the trend of the ionization yield *vs.* energy. At low to moderate photon energies, the singly ionized intensity increases until it reaches very close to 100% quantum yield. This occurs around 30 eV (see Fig. 4). Around 45 eV, the second ionization appears and begins to deplete the singly ionized species, reducing the measured signal (see Fig. 3). This is 5–10 eV below the energy where the ions start to fragment by C_2 loss on a time scale given by the acceleration time in the time-of-flight mass spectrometer, which is on the order of a microsecond.

The measured electron yield is calculated quantitatively as the time-integrated production rate multiplied by the survival probability:

$$P_1 = \int_0^{\infty} P_0(t)k_0(E(t))P_1'(t)dt, \quad (7)$$

where, in analogy to eqn (6), the factor

$$P_1'(t) \equiv \exp\left(-\int_0^{\infty} k_1(E(t')e^{-t'/\tau})dt'\right), \quad (8)$$

is the survival probability of the singly charged ion created with energy $E(t) = h\nu e^{-t/\tau} - \Phi$ at time t . Inserting the expressions for the functions, the equation becomes

$$P_1 = \int_0^t \exp\left(-\int_0^{\infty} k_0(h\nu e^{-t'/\tau})dt'\right)k_0(h\nu e^{-t/\tau}) \times \exp\left(-\int_0^{\infty} k_1\left(\left(h\nu e^{-t'/\tau} - \Phi\right)e^{-t'/\tau}\right)dt'\right)dt \quad (9)$$

As can be seen from Fig. 6, the decrease with photon energy is not completed before around 80 eV. We should stress here that the curve gives the expected abundance of singly charged ions after the absorption of one photon that generated the hot electron state. The cross section for this absorption is not known at present. An experimentally measured yield and this

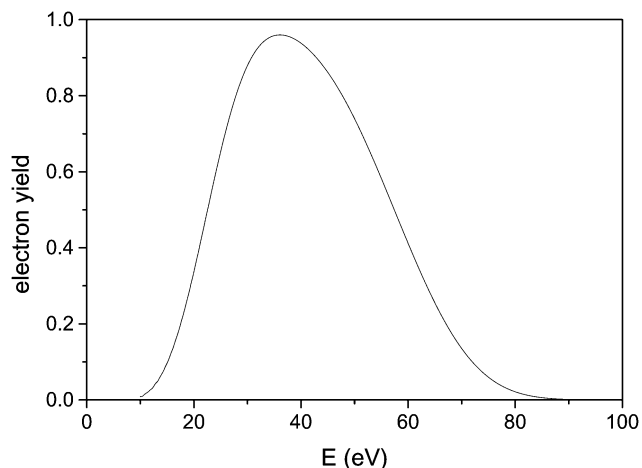


Fig. 6 Ionization yield, calculated with eqn (9), giving the total yield of the singly ionized species.

curve will provide this (relative) cross section, to the extent the model presented here is reliable.

One way of verifying or falsifying the model is by comparing calculated and experimentally measured kinetic energy distributions. These were calculated for each photon energy, f_i , by inserting the normalized branching ratio, $f_i(E, \varepsilon)$, under the integral sign in eqn (7):

$$f_i(\varepsilon) = \int_0^\infty P_0(t)k_0(t)f(E(t), \varepsilon)P_1'(t)dt$$

$$\propto \int_0^\infty P_0(t)k_0(t)c'\sigma(\varepsilon)\varepsilon\rho_d(h\nu e^{-t/\tau} - \Phi - \varepsilon)P_1'(t)dt.$$
(10)

The results of integration of this are shown in Fig. 7 for several photon energies. The curves all display a negative curvature on a logarithmic scale, consistent with the general behavior of the

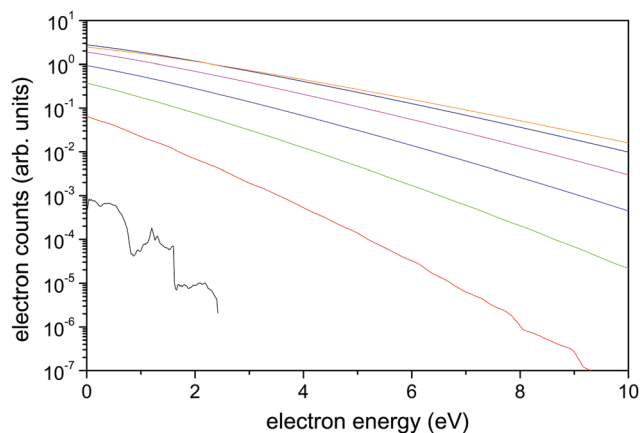


Fig. 7 Simulated kinetic energy distributions for the photon energies 10 to 70 eV in steps of 10 eV. The curves are shifted a factor three up for each new and higher photon energy. The photon energies were, as before 10 eV (black line), 20 eV (red line), 30 eV (green line), 40 eV (blue line), 50 eV (magenta line), 60 eV (navy line), and 70 eV (orange line). The distributions only include the singly ionized species.

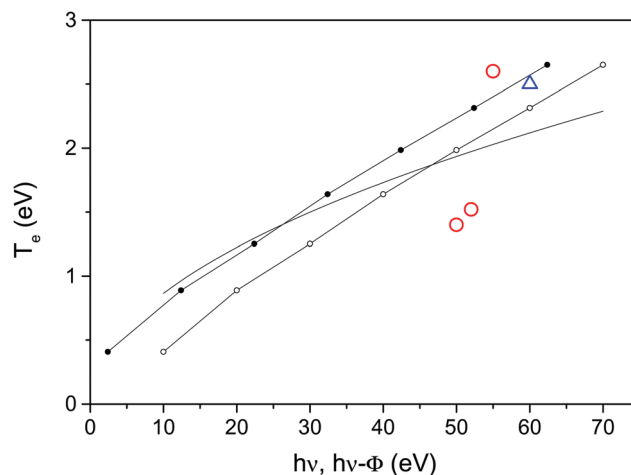


Fig. 8 Simulated and observed temperatures. The simulated values were calculated as the reciprocal of the simulated kinetic energy spectra shown in Fig. 7 vs. the photon energy (open circles) and the same temperatures vs. the photon energy minus the ionization energy. The full line is the behavior expected for a Fermi gas. The large open red circles give the experimentally observed values in coincidence with C_{58}^+ , and the triangle the value measured with C_{56}^+ as the final product.

level densities, although the energies are not an exact mapping of this function, as should be clear from eqn (2) and the time dependence of T_e . The logarithmic slope decreases with increasing photon energy, as expected. The total intensities increase and then decrease, as expected from Fig. 6.

The fitted temperature from the lowest 2 eV of the calculated electron spectra is shown in Fig. 8 for the photon energies used in the previous figures. The curve is close to linear, albeit with an offset, contrary to a naive expectation for a Fermi-gas caloric curve, which would be a square root behavior. The values are shown both vs. the photon energy and the photon energy minus the ionization energy, which corresponds to the excitation energy of the product. This is expected to give a better comparison with the expected values (see eqn (2)). The line gives the best fit square root, which is the caloric curve of a Fermi-gas, $T = \sqrt{aE}$. This is seen to fit rather poorly. The value of the fit parameter a in the equation is 0.075 eV. In terms of the average level spacing at the Fermi energy, Δ , this corresponds to $\Delta = \pi^2/6 \times 0.075 \text{ eV} = 0.12 \text{ eV}$.³⁷ This should be compared with the expected value $\Delta_{\text{FG}} = (30 - 7.6)/N_e \times 3/2 = 0.14 \text{ eV}$, for 240 valence electrons and a depth of the 3-d Fermi sea of 30 eV. The agreement is comforting and better than can be expected from the quality of the fit. The discrepancy does suggest, however, that the kinetic energy distributions need to be calculated explicitly in the analysis of experiments.

The comparison of measured temperatures to those predicted by the model presented here is potentially complicated by the presence of the surface plasmon resonance. This resonance, which is known to account for a significant part of the dipole oscillator strength, peaks at 20 eV and decreases beyond this energy with a very broad profile. This is likely to cause some distortion of the slope in the region where the plasmon is present. The comparison here is therefore only made at higher photon energies. The total

excitation energy is so high that the ions produced will undergo fragmentation later, as explained above, and only electrons measured in coincidence with $C_{56,58}^+$ are observed at these energies. This has the added advantage that it removes the background from the directly ionized molecules. The simulations reproduce the coarse features of the data points, as seen in Fig. 8, but there are also significant deviations. The origin of these deviations is not known at the moment and more experimental work is required to cast light on this question.

4 Discussion and perspectives

In this article, several signals have been calculated for the characterisation of the emission of electrons from a single-photon excited hot electron gas. The calculations are based on a model which previously has been found to give a good representation of the analogous process after multiphoton absorption by C_{60} . The target molecule was chosen for two reasons: it can be put into the gas phase as a very pure species. Hence we know the precursor for observed ions in the coincidence experiments, and secondly, that the breakdown of the molecule at high excitation energy is very well known, and that the threshold is located high in energy compared to a smaller molecule composed of, say, five or 10 atoms. For C_{60} , all decay channels that occur on the nanosecond and longer time scales are well-characterized, permitting a safe identification of the ionization mechanism. We expect that the observations made on C_{60} will find their parallel in other systems. Studies are already under way to investigate this question. The observation of hot electron emission following the absorption of a single photon is not only remarkable as a novel ionization mechanism. The fact that the excitation is achieved with a very well defined energy, as opposed to the multiphoton processes that by nature require extensive averaging,³⁸ permits a much closer scrutiny of the process when combined with future, more detailed experimental results.

Acknowledgements

Conversations with V. Zhaunerchyk and R. Feifel are gratefully acknowledged.

References

- 1 F. Reinert and S. Hüfner, *New J. Phys.*, 2005, **7**, 97.
- 2 J. V. Coe, S. M. Williams and K. H. Bowen, *Int. Rev. Phys. Chem.*, 2008, **27**, 27–51.
- 3 K. Siegbahn, C. Nordling, G. Johansson, J. Hedman, P. F. Hedén, K. Hamrin, U. Gelius, L. O. Werme, R. Manne and Y. Baer, *ESCA Applied to Free Molecules*, North-Holland, 1969.
- 4 P. Agostini, F. Fabre, G. Mainfray, G. Petite and N. K. Rahman, *Phys. Rev. Lett.*, 1979, **42**, 1127.
- 5 W. Becker, F. Grasbon, R. Kopold, D. B. Milosevic, G. G. Paulus and H. Walther, *Adv. At., Mol., Opt. Phys.*, 2002, **48**, 35.
- 6 R. R. Freeman, P. H. Bucksbaum, H. Milchberg, S. Darack, D. Schumacher and M. E. Geusic, *Phys. Rev. Lett.*, 1987, **59**, 1092.
- 7 T. Leisner, K. Athanassenas, O. Echt, O. Kandler, D. Kreisle and E. Recknagel, *Z. Phys. D: At., Mol. Clusters*, 1991, **20**, 127.
- 8 P. Wurz and K. R. Lykke, *J. Chem. Phys.*, 1991, **95**, 7008.
- 9 E. E. B. Campbell, G. Ulmer and I. V. Hertel, *Phys. Rev. Lett.*, 1991, **67**, 1986.
- 10 G. Ganteför, W. Eberhardt, H. Weidele, D. Kreisle and E. Recknagel, *Phys. Rev. Lett.*, 1996, **77**, 4524.
- 11 J. M. Weber, K. Hansen, M.-W. Ruf and H. Hotop, *Chem. Phys.*, 1998, **239**, 271.
- 12 K. Hansen, Proceedings of ‘Similarities and Differences Between Atomic Nuclei and Clusters’, Tsukuba, Japan, July 1997; Y. Abe, I. Arai, S. M. Lee and K. Yabana, (ed.), AIP Conf. Proc., New York, 1998.
- 13 E. E. B. Campbell, K. Hansen, K. Hoffmann, G. Korn, M. Tchapyguine, M. Wittmann and I. V. Hertel, *Phys. Rev. Lett.*, 2000, **84**, 2128–2131.
- 14 M. Kjellberg, O. Johansson, F. Jonsson, A. V. Bulgakov, C. Bordas, E. E. B. Campbell and K. Hansen, *Phys. Rev. A: At., Mol., Opt. Phys.*, 2010, **81**, 023202.
- 15 R. Schlipper, R. Kusche, B. v. Issendorff and H. Haberland, *Appl. Phys. A: Mater. Sci. Process.*, 2001, **72**, 255.
- 16 N. Pontius, G. Lüttgens, P. S. Bechthold, M. Neeb and W. Eberhardt, *J. Chem. Phys.*, 2001, **115**, 10479–10483.
- 17 M. Maier, M. Astruc Hoffmann and B. v. Issendorff, *New J. Phys.*, 2003, **5**, 3.1.
- 18 K. Hansen, K. Hoffmann and E. E. B. Campbell, *J. Chem. Phys.*, 2003, **119**, 2513–2522.
- 19 M. Kjellberg, A. V. Bulgakov, M. Goto, O. Johansson and K. Hansen, *J. Chem. Phys.*, 2010, **133**, 074308.
- 20 T. Laarmann, M. Rusek, H. Wabnitz, J. Schulz, A. R. B. de Castro, P. Gürtler, W. Laasch and T. Möller, *Phys. Rev. Lett.*, 2005, **95**, 063402.
- 21 M. Perner, S. Gresillon, J. Marz, G. von Plessen, J. Feldmann, J. Porstendorfer, K. J. Berg and G. Berg, *Phys. Rev. Lett.*, 2000, **85**, 792–795.
- 22 D. W. Forslund, J. M. Kindel and K. Lee, *Phys. Rev. Lett.*, 1977, **39**, 284–288.
- 23 J.-Y. Bigot, J.-Y. Merle, O. Cregut and A. Daunois, *Phys. Rev. Lett.*, 1995, **75**, 4702–4705.
- 24 V. Weisskopf, *Phys. Rev.*, 1937, **52**, 295.
- 25 N. Bohr, *Science*, 1937, **86**(2225), 161–165.
- 26 K. Hansen, R. Richter, M. Alagia, S. Stranges, L. Schio, P. Salén, V. Yatsyna, R. Feifel and V. Zhaunerchyk, *Phys. Rev. Lett.*, 2017, **118**, 103001.
- 27 F. Lépine and C. Bordas, *Phys. Rev. A: At., Mol., Opt. Phys.*, 2004, **69**, 053201.
- 28 K. Hansen and O. Echt, *Phys. Rev. Lett.*, 1997, **78**, 2337.
- 29 R. Deng, G. Littlefield and O. Echt, *Z. Phys. D: At., Mol. Clusters*, 1997, **40**, 355.
- 30 P. O’Keeffe, P. Bolognesi, M. Coreno, A. Moise, R. Richter, G. Cautero, L. Stebel, R. Sergo, L. Pravica, Y. Ovcharenko and L. Avaldi, *Rev. Sci. Instrum.*, 2011, **82**, 033109.

- 31 A. T. J. B. Eppink and D. H. Parker, *Rev. Sci. Instrum.*, 1997, **68**, 3477–3484.
- 32 G. A. Garcia, L. Nahon and I. Powis, *Rev. Sci. Instrum.*, 2004, **75**, 4989.
- 33 B. Dick, *Phys. Chem. Chem. Phys.*, 2014, **16**, 570.
- 34 K. Yabana and G. F. Bertsch, *Phys. Scr.*, 1993, **48**, 633.
- 35 F. C. Williams, *Nucl. Phys. A*, 1969, **133**, 33.
- 36 M. Brack, O. Genzken and K. Hansen, *Z. Phys. D: At., Mol. Clusters*, 1991, **21**, 65.
- 37 K. Hansen, *Statistical Physics of Nanoparticles in the Gas Phase*, Springer, Dordrecht, 2013.
- 38 K. Mehlig, K. Hansen, M. Hedén, A. Lassesson, A. V. Bulgakov and E. E. B. Campbell, *J. Chem. Phys.*, 2004, **120**, 4281.